Int. J. Heat Mass Transfer. Vol. 25, No. 2, pp. 195–203, 1982
Printed in Great Britain

0017–9310/82/020195–09 $03.00/0

HEAT TRANSFER IN CURVED TUBES WITH PULSATING FLOW

N. J. RABADI
Gard Inc., Niles, IL 60648, U.S.A.

and

J. C. F. CHOW and H. A. SIMON
University of Illinois, Box 4348, Chicago, IL 60680, U.S.A.

(*Received* 28 *January* 1981 *and in revised form* 19 *June* 1981)

Abstract—Effects of pulsatile flow upon heat transfer characteristics are studied for fully developed, laminar, and pulsating flow in curved tubes. The heat transfer boundary conditions are taken to be axially uniform heat flux with peripherally uniform wall temperature. Temperature distribution, and local and peripherally averaged Nusselt numbers are calculated for different values of frequency and amplitude ratio parameters, Reynolds number, curvature ratio, Dean and Prandtl numbers. The result shows that there is considerable variation in local and peripherally averaged Nusselt number. The time and space averaged Nusselt number approaches the corresponding steady state flow case at frequency parameter $\alpha = 6$ and decreases as α decreases. A further decrease is associated with increasing amplitude ratio at low frequencies.

NOMENCLATURE

a, tube radius;
De, Dean number $= Re/\sqrt{R_o}$
k, (RAT), ratio of the maximum amplitude of the oscillating pressure gradient to the steady component;
K, fluid thermal conductivity;
n, dimensionless temperature;
Nu_l, local Nusselt number defined in terms of the time averaged mean temperature;
$\overline{Nu}$, peripherally averaged Nusselt number;
$\overline{\overline{Nu}}$, time and space averaged Nusselt number;
P, dimensionless pressure, $= P'a^2/\rho\nu^2$;
Pr, Prandtl number;
Re, Reynolds number based on tube radius and the average axial velocity resulting from the steady pressure gradient P_{st};
R_o, dimensionless tube radius of curvature, $= R'_0/a$;
R, dimensionless toroidal radius, $= R'/a$;
r, dimensionless radial coordinate in tube, $= r'/a$;
T, temperature, fraction of a cycle;
t, time, $= \omega t'$;
W, dimensionless axial velocity component, $= aW'/\nu$.

Greek symbols

α, frequency parameter, $a\sqrt{\omega/\nu}$;
ω, frequency of pulsation;
θ, angular coordinate in plane of tube curvature;
μ, dynamic viscosity;
ν, kinematic viscosity;
ξ, dimensionless axial vorticity component;
ρ, density;
ϕ, angular coordinate of tube cross-section;
ψ, dimensionless secondary stream function;
$\Delta\psi$, change in ψ between adjacent secondary stream lines;
Δn, change in n between adjacent isotherms;
$'$, denotes dimensional variable.

Subscripts

l, local;
w, at the wall;
st, steady component.

INTRODUCTION

ALTHOUGH pulsating flow in curved tubes occurs frequently in both natural phenomena and engineering systems, very little related work is available in the literature, and consequently the problem is not completely understood.

It was only quite recently that Lyne [1] initiated the analysis of unsteady pulsatile flows in curved tubes. The motion induced in a circular tube by a sinusoidally time-varying pressure gradient with zero mean is assessed. He predicts additional secondary circulation of opposite direction to that of steady flow in the inviscid core and postulates that this additional secondary flow is due to shear action.

Zalosh and Nelson [2] use the Finite Hankel Transform to obtain analytical solutions for a medium range of the frequency parameter α.

Chow and Li [3] employ the same technique used by Zalosh and Nelson, but their solution covers a wider range of α. They find that the secondary flow patterns vary with respect to α and can be divided into three distinct phases dictated by the relative importance of the viscous and inertia forces: (1) the shear force dominated flow with a single circulation, (2) the

transitional flow with either one or two circulations, and (3) the boundary layer flow with either one or two circulations, and (3) the boundary layer flow with two circulations. They confirm Lyne's [1] prediction of the formation of an additional circulation in the inviscid core but they report that it is more likely to be due to inertia forces, rather than shear action as postulated by Lyne.

Simon *et al.* [4] use a perturbation analysis including the second-order solution for fluid and heat transfer. The results obtained cover a wide range of excitation parameters ($\alpha = 0.1$–12, $k = 0.01$–3) and Prandtl number ($Pr = 1.0$–100), but small Dean number ($De < 22$). Their results show that the increase in the time averaged Nusselt number are most evident at high Prandtl numbers, high excitation relative amplitudes, and low excitation frequencies. They report that the Nusselt number ratio (curved pulsatile to straight pulsatile) passes through a maximum value at low α. This unusual result is negated by the more exact numerical solution results described in the body of the current paper. It can be inferred that the pertubation analysis, limited as it is to solutions of the second-order, is unable to describe fully the details of the secondary flow phenomena in pulsatile flow especially at low excitation frequency.

Conflicting results have been reported for the pulsating flow and heat transfer in straight tubes. In some cases the flow pulsations seem to enhance the heat transfer, whereas, in other cases either no significant effect is shown or a decrease occurs.

The solutions for pure oscillatory and pulsatile flows available in the literature are mostly analytical and restricted to very low Dean numbers (< 22).

The purpose of the present study is to magnify the secondary flow effect, by extending the Dean number range, and to show the outcome of the interaction between the flow pulsations and the secondary flow. The effect of this interaction on the heat transfer is discussed. The energy equation is solved using the velocity distribution results reported in an earlier paper by Rabadi *et al.* [5] and in full in a Ph.D. thesis [6]. The numerical techniques used are the same as those employed by Rabadi *et al.* [5].

FORMULATION OF THE PROBLEM

Consider a circular tube of radius a coiled in a circle of radius R_0 about the axis OZ as shown in Fig. 1. The curved tube could be thought of as a part of a helical tube with zero pitch. The system of coordinates shown in Fig. 1 is a toroidal coordinate system. Any point inside the tube can be completely located by specifying the three orthogonal toroidal coordinates θ, ϕ and r.

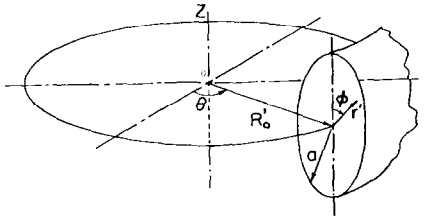

FIG. 1. System of toroidal coordinates for a circular tube.

The present analysis concerns pulsatile laminar flow and heat transfer in curved tubes. The following assumptions are made:

(1) the fluid behaves like an incompressible, viscous Newtonian fluid with constant properties;
(2) both the laminar flow and the temperature fields are fully developed;
(3) the effects of free convection and viscous dissipation are negligible;
(4) axial conduction is negligible relative to radial conduction;
(5) the coil pitch effect is negligible.

The effects of free convection have been studied by Singh and Bell [7] and Abul-Hamayel [8] experimentally, and Yao and Berger [9] analytically using perturbation methods. These studies show that the effects of free convection can be of significance at low Reynolds number. Thus, the present study is limited to small Grashof numbers when the Reynolds number is small.

The dimensionless equations (1–3) governing the flow are [Kalb [1973)]:

axial velocity, W, equation:

$$\alpha^2 \frac{\partial W}{\partial t} + AW + B\frac{\partial W}{\partial \phi} + C\frac{\partial W}{\partial r} + \frac{\partial^2 W}{\partial r^2} - \frac{1}{r^2}\frac{\partial^2 W}{\partial \phi^2} = \frac{1}{R}\frac{\partial P}{\partial \theta}(1 + k\cos t),$$

axial vorticity, ξ, equation:

$$\alpha^2 \frac{\partial \xi}{\partial t} + A_\xi \xi + B\frac{\partial \xi}{\partial \phi} + C\frac{\partial \xi}{\partial r} - \frac{\partial^2 \xi}{\partial r^2} - \frac{1}{r^2}\frac{\partial^2 \xi}{\partial \phi^2} = D_W$$

where ξ is defined as

$$\xi = \left(\frac{1}{rR} - \frac{\sin\phi}{R^2}\right)\frac{\partial \psi}{\partial r} + \frac{1}{R}\frac{\partial^2 \psi}{\partial r^2} - \frac{\cos\phi}{rR^2}\frac{\partial \psi}{\partial \phi} + \frac{1}{r^2 R}\frac{\partial^2 \psi}{\partial \phi^2}.$$

The coefficients, A, A_ξ, B and C are functions of the space variables r, R and ϕ, and first-order stream function derivatives. D_W is a function of the space variables as well as the axial velocity W and its derivatives.

$$A_\xi = \frac{1}{R^2}\left(1 - \cos\phi\frac{\partial \psi}{\partial r} + \frac{\sin\phi}{r}\frac{\partial \psi}{\partial \phi}\right),$$

$$B = \frac{1}{rR}\left(\frac{\partial \psi}{\partial r} - \cos\phi\right),$$

$$C = -\left(\frac{1}{r} + \frac{\sin\phi}{R} + \frac{1}{rR}\frac{\partial \psi}{\partial \phi}\right),$$

$$A = \frac{1}{R^2}\left(1 + \cos\phi\frac{\partial \psi}{\partial r} - \frac{\sin\phi}{r}\frac{\partial \psi}{\partial \phi}\right),$$

$$D_W = 2\frac{W}{R}\left(\cos\phi\frac{\partial W}{\partial r} - \frac{\sin\phi}{r}\frac{\partial W}{\partial \phi}\right);$$

α is referred to as 'the frequency parameter.' Other researchers refer to α as the oscillatory Reynolds

number. In fact, α^2 is the ratio of the characteristic diffusion time, a^2/ν to the characteristic oscillatory time, $1/\omega$.

The axial pressure gradient, which is the only pressure term that explicitly appears in the final equations is expressed as follows:

$$\frac{\partial P}{\partial \theta} = \left(\frac{\partial P}{\partial \theta}\right)_{st} (1 + k \cos t).$$

This assumes that the driving force is a sinusoidally time varying axial pressure gradient imposed on a steady component $(\partial P/\partial\theta)_{st}$. The ratio of the maximum amplitude of time varying component to the steady component is k.

The heat transfer boundary condition chosen in this work assumes that the wall temperature T_w varies linearly in the axial direction but is uniform peripherally and constant with time.

A non-dimensional temperature n is defined in the following form:

$$n = \frac{(T_w - T)}{a(\partial T/\partial\theta)} R_o$$

where $\partial T/\partial\theta$ is constant for a thermally fully developed flow.

The dimensionless energy equation is [10]:

$$-Pr\alpha^2 \frac{\partial n}{\partial t} + B_T \frac{\partial n}{\partial \phi} + A_T \times \frac{\partial n}{\partial r} + \frac{\partial^2 n}{\partial r^2} + \frac{1}{r^2}\frac{\partial^2 n}{\partial \phi^2} = \frac{WR_o}{R}$$

where

$$A_T = \frac{1}{r} + \frac{\sin\phi}{R} + \frac{Pr}{rR}\frac{\partial \psi}{\partial \phi},$$

$$B_T = \frac{\cos\phi}{rR} - \frac{Pr}{rR}\frac{\partial \psi}{\partial r},$$

and Pr is the Prandtl number, $\mu C_p/K$.

Boundary conditions

Figure 2 illustrates the boundary conditions. Four regions are identified separately: (1) tube wall where $W = \psi = n = 0$, $\xi = -R^{-1}(\partial^2\psi/\partial r^2)$, (2) left horizontal radius where $\psi = \xi = 0$, $\partial W/\partial\phi = \partial n/\partial\phi = 0$, (3) right horizontal radius where $\psi = \xi = 0$, $\partial\psi/\partial\phi = \partial n/\partial\phi = 0$, and (4) center point where $\psi = \xi = 0$, $\partial W/\partial r = \partial n/\partial r = 0$.

RESULTS AND DISCUSSION

As defined before, the dimensionless temperature represents the difference between the tube wall and the fluid temperature. The temperature profiles are shown for the upper half of the tube cross-section, in the form of contours. A fixed number of contours (10) is adopted in all the plots. This means that different values of Δn (the difference in dimensionless temperature between neighboring contour lines) are adopted for each plot. Therefore, the large spacing between the contours represent areas of relatively flat temperature gradients, whereas places where the contour lines are close together represent steep temperature gradients. These temperature contour plots are very useful for visualizing the effects that various parameters have on the temperature field. Note that for either heating or cooling, the dimensionless temperature is zero at the wall. Extrema on these contour plots correspond to the highest and lowest fluid temperatures. The $\oplus$ and $\ominus$ signs are for positive and negative dimensionless temperatures, respectively.

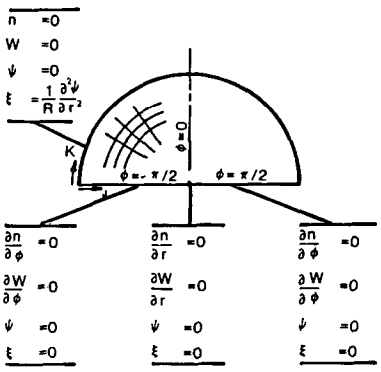

FIG. 2. Boundary conditions.

Each of these temperature contour plots represents the profiles at four different times during a cycle (T = 0.25, 0.5, 0.75 and 1.0). These times are the same at which the axial velocity profiles, and the secondary flow stream lines are given.

Figure 3 shows the variations of axial velocity at four times during a cycle for α = 2, 4 and 10, and k = 1.5. The maximum velocity is moved towards the outside of the pipe, as in steady flow. The steep velocity gradient created in this region is instrumental in increasing the heat transfer as will be seen later. The higher the frequency the less the flow responds to the pulsating pressure. At low frequency (α = 2.0) the response is a maximum, and a flow reversal actually occurs at T = 0.25.

The secondary flows induced at corresponding times in the cycle are shown in Fig. 4. Further details of the flow are available in an earlier publication by Rabadi *et al.* [5]. The intensity of the secondary flow is revealed by the value of $\Delta\psi$ (the change in the streamfunction between adjacent streamlines). The flow moves rapidly along the periphery from outside to inside, with a slower return along the pipe diameter which is an axis of symmetry for the upper and lower circulations. For the case illustrated in Fig. 4. the circulation is most intense at T = 0.75 and reduces by an order of magnitude during the cycle. At its strongest the return flow resembles a jet flowing from the outside ($\phi = \pi/2$) around the periphery.

The secondary flows have a profound and interesting effect on the temperature distributions. It is clear in Figs. 5 and 6 that for a high Prandtl number (Pr = 5), convection effects are dominant. The high tempera-

tures near the wall at the outside of the duct are carried across the pipe center line by the secondary flows. This creates two minimum temperature regions, one in each half of the pipe. The effect is greatly reduced for $\alpha = 2$, when $T = 0.25$ and 0.5 (Fig. 6), as during this portion of the cycle the secondary flow has been greatly reduced (Figs. 3 and 4). In reading these figures the value of Δn should be observed as it represents the temperature change between adjacent isotherms. At $\alpha = 10.0$ (Fig. 5), Δn changes little during a cycle. However at $\alpha = 2.0$ (Fig. 6), it changes considerably, reflecting the relative intensity of the secondary flow at different times during the cycle.

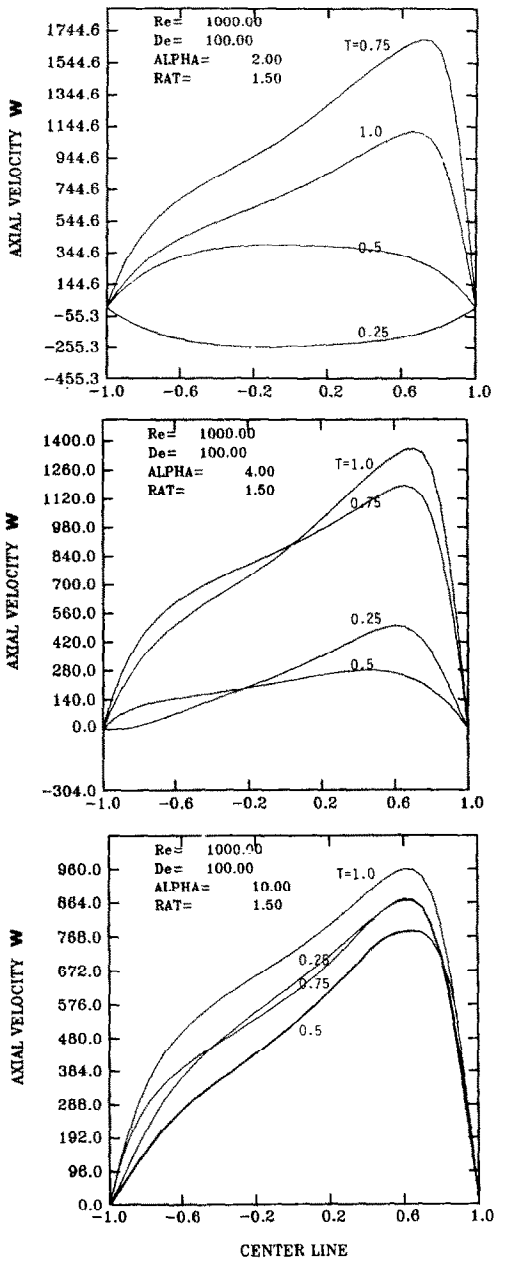

FIG. 3. Axial velocity distributions on horizontal diameter for $\alpha = 2, 4$ and $10, k = 1.5, Re = 1000, De = 100$ and fractions of a cycle $T = 0$ (1.0), 0.25, 0.5 and 0.75.

For very small Prandtl numbers (not shown) conduction dominates and the isotherms tend towards concentric circles about the pipe center, greatly reducing the effects of curvature.

Figure 7 illustrates an intermediate Prandtl number ($Pr = 0.7$). In this case convection is sufficient to move the minimum towards the outside of the pipe, when the

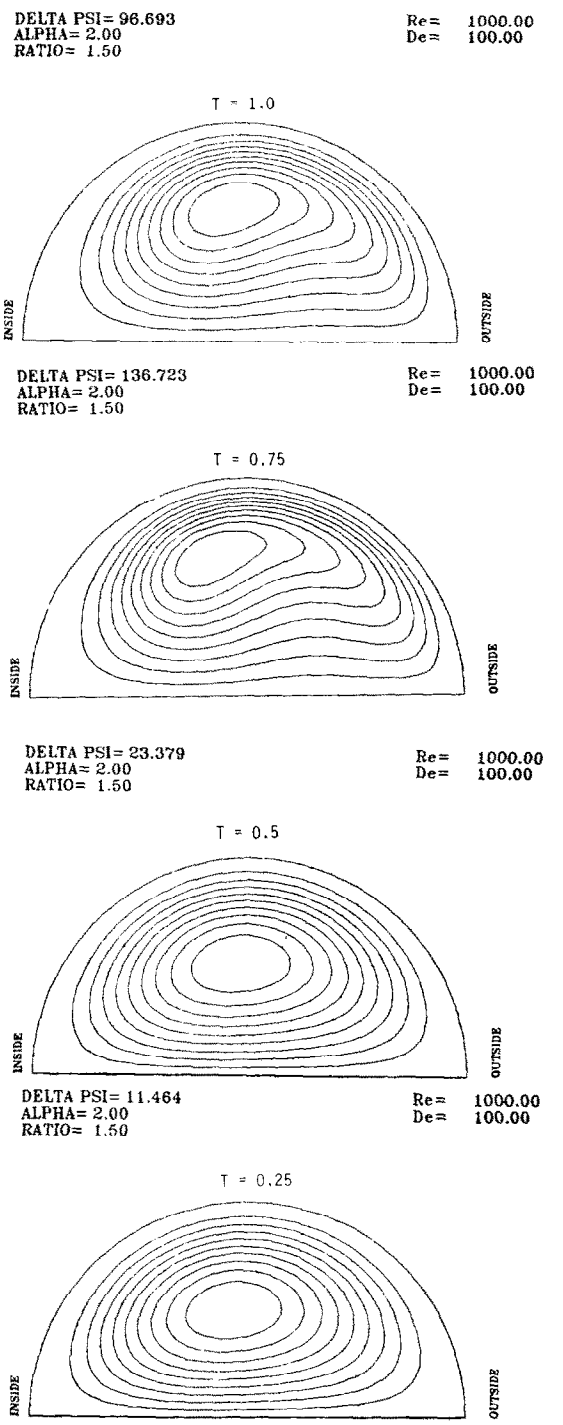

FIG. 4. Secondary flow streamlines for $\alpha = 2.0, k = 1.5, Re = 1000, De = 100$ and fractions of a cycle $T = 0$ (1.0), 0.25, 0.5 and 0.75.

secondary flow is not intense, but not sufficient to form the bi-modal distribution discussed above. Again, when $T = 0.25$ and 0.5 the patterns change considerably because of the reduction of axial velocity and the associated secondary flows. At $T = 0.25$ a small temperature maximum occurs towards the inside of the pipe because of the flow reversal in the axial direction. The steep temperature gradients, evident at the outside of the duct and the adjacent peripheral region in Figs. 5–7, give rise to enhanced Nusselt numbers in these regions. These increased values are partly offset by the decreased Nusselt numbers associated with the reduced gradients seen at the inside

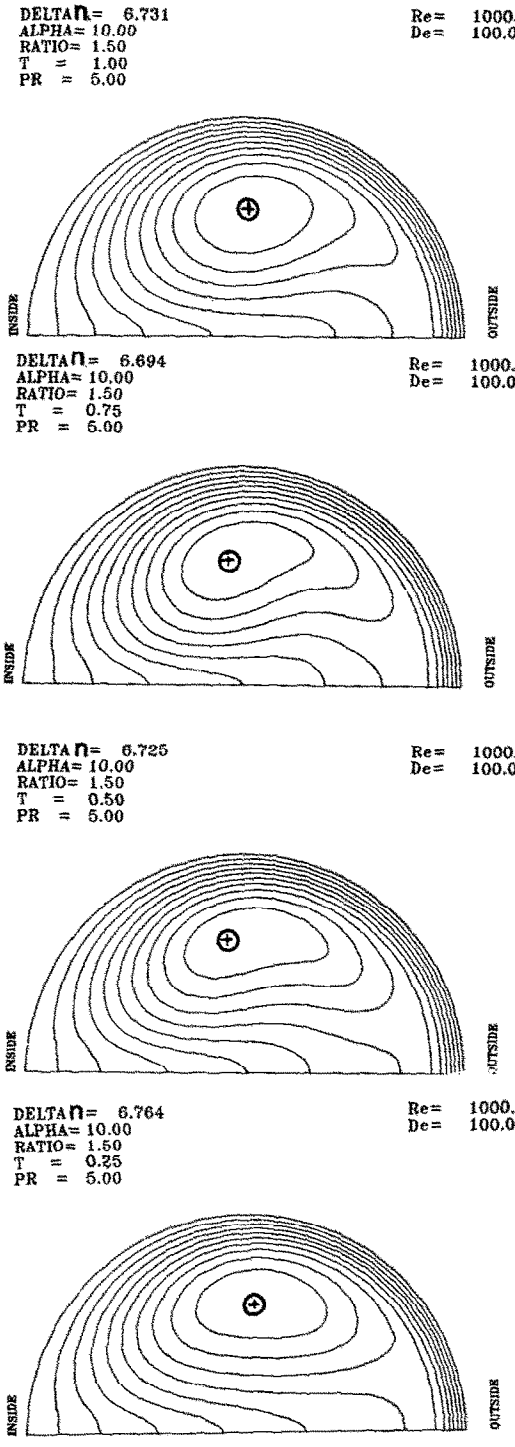

FIG. 5. Isotherms for $\alpha = 10.0$, $k = 1.5$, $Pr = 5.0$, $Re = 1000$, $De = 100$ and fractions of a cycle $T = 0$ (1.0), 0.25, 0.5 and 0.75.

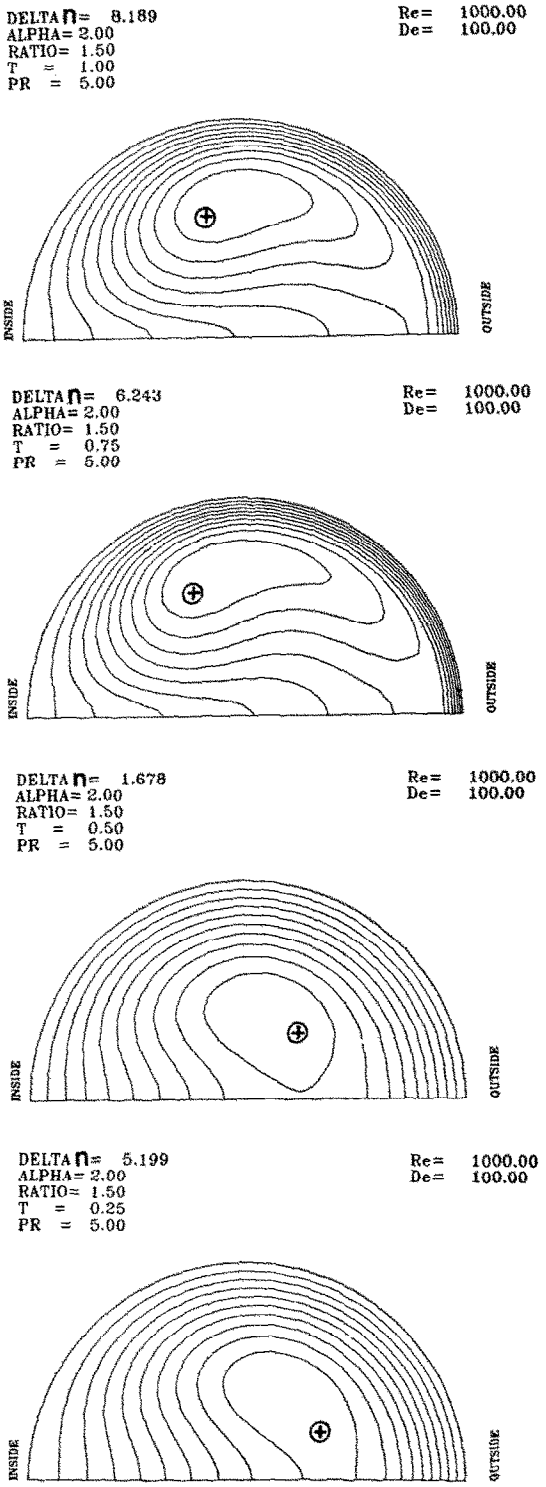

FIG. 6. Isotherms for $\alpha = 2.0$, $k = 1.5$, $Pr = 5.0$, $Re = 1000$, $De = 100$ and fractions of a cycle $T = 0$ (1.0), 0.25, 0.5, and 0.75.

of the duct. Reduced gradients are particularly evident for $\alpha = 2$ at $T = 0.25$ and 0.5 (Figs. 3 and 7) as the pulsations reduce the intensity of the secondary flow. Ultimately, as shown below, this leads to a reduction in the time and space averaged values of the Nusselt number as compared with higher values of α.

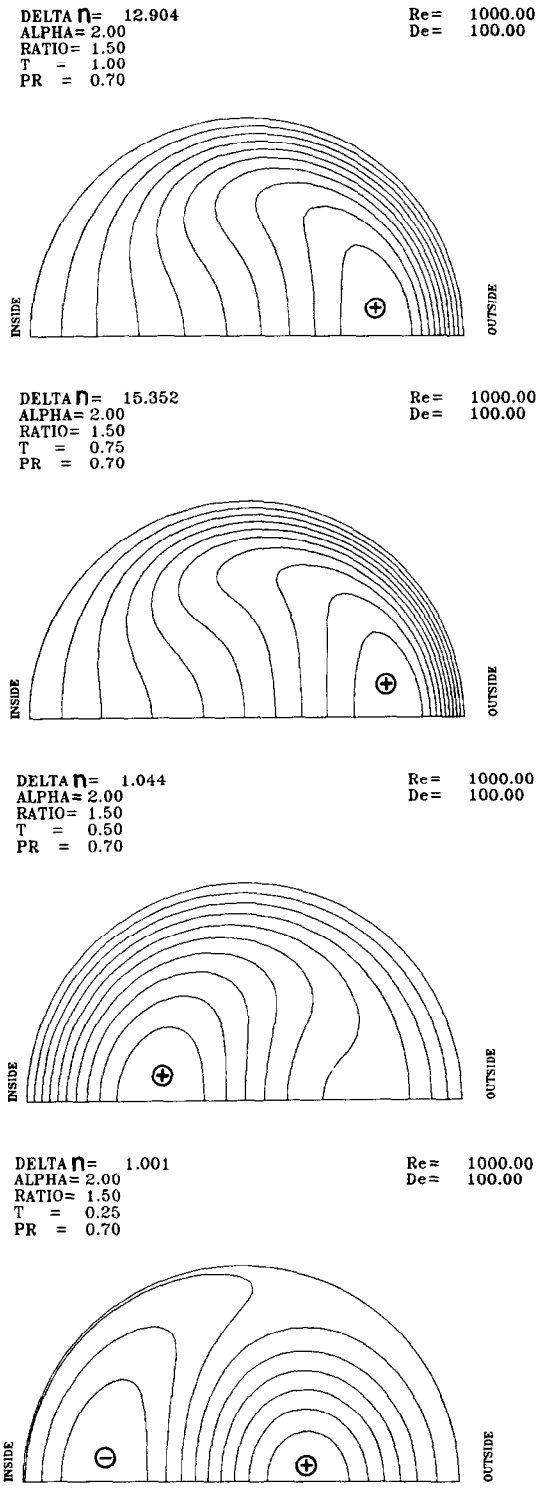

FIG. 7. Isotherms for $\alpha = 2.0, k = 1.5, Pr = 0.7, Re = 1000, De = 100$ and fractions of a cycle $T = 0$ (1.0), 0.25, 0.5 and 0.75.

Figures 8–10 illustrate the local distribution of Nusselt number, Nu_l, around the periphery as well as the peripherally averaged Nusselt number, $\overline{Nu}$, as a function of time. An angle of 90° refers to the outside of the pipe and −90° to the inside. For $\alpha = 10$ and $Pr = 5$, not only is the heat transfer convection dominated, but secondary flows vary little during the cycle. Nu_l is highest at the outside of the pipe due to strong secondary flows revealing a boundary layer type of build-up, originating at that point. For $\alpha = 2$, Figs. 9 and 10, Nu_l varies widely during a cycle at the outside wall because of the diminution of the secondary flow for $T = 0.25$ and 0.5. Figures 8–10 also show a change in the phasing of $\overline{Nu}$ in time. At low frequency, viscous forces predominate and the forcing function and the velocity response are in phase. At higher frequencies inertial forces predominate and the forcing function and velocity become 90° out of phase. This phased reaction is duplicated by $\overline{Nu}$ which responds with the velocity. Slight irregularities in the smoothness of the curves (see Figs. 9 and 10 for example) were checked by repeating the numerical analysis for smaller grid sizes and time steps. The irregularities were found to be

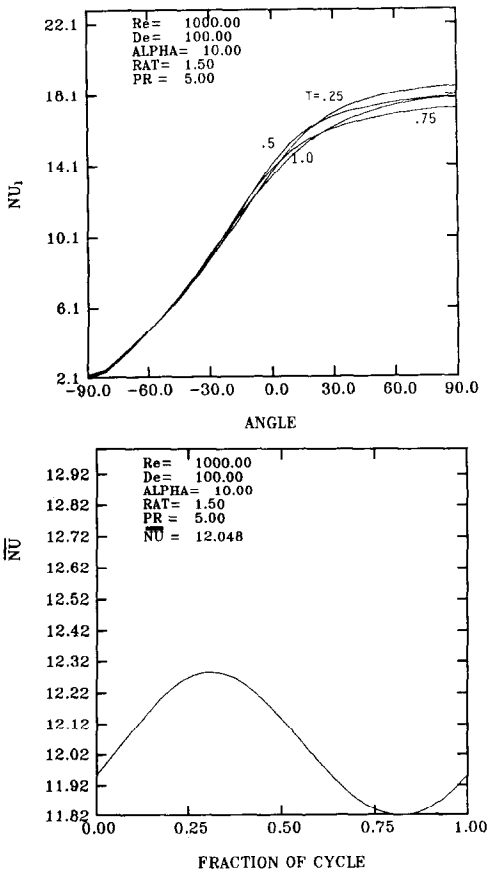

FIG. 8. Local Nusselt number Nu_l as a function of angle ϕ ($\phi = 90°$ at outside of horizontal diameter) and for $T = 0$ (1.0), 0.25, 0.5, 0.75 and peripherally averaged Nusselt number $\overline{Nu}$ as a function of cycle fraction, for $\alpha = 10.00, k = 1.5, Pr = 5.0, Re = 1000$ and $De = 100$.

stable and hence were not the outcome of numerical procedures.

The Prandtl number always plays an important role when boundary layer phenomena are involved, and this is most evident in Figs. 11–13, which show the behavior of the time and peripherally averaged Nusselt number $\overline{Nu}$. At the Dean number shown ($De = 100$), $Pr = 0.5$ and 0.005 give almost identical results. This implies that the heat transfer is conduction dominated with respect to the secondary flows. As α reduces, $\overline{Nu}$ reduces because of variations in axial velocity. This reduction is clearly more pronounced as k increases from 0.5 to 1.0 to 1.5. Convection, resulting from the secondary flows, leads to a pronounced increase in $\overline{Nu}$ as the Prandtl number increases.

The Nusselt number results for the frozen conditions (high α), can be compared to the steady state solution available in the literature. Table 1 lists the value of the time averaged peripherally averaged Nusselt number at high frequency for the present work compared with the steady state results of Kalb [10]. Excellent agreement is shown for low Prandtl number. For $Pr = 5$ the effect of secondary flow becomes more important, hence higher α is needed to assure thermally frozen conditions.

The results presented here do not show the same behavior as that predicted in an earlier paper by Simon *et al.* [4], for small values of α. It must be concluded that the perturbation analysis used there up to the second order, is simply not able to model accurately the complex secondary flows that occur at low α.

CONCLUSIONS

In laminar, pulsatile, curved tube flows, the Nusselt number varies widely both around the tube periphery and also during a cycle. These effects are greatest for large Prandtl numbers and small values of the frequency parameter α. The time and space averaged Nusselt number is large for large Prandtl numbers and falls at low values of α. This latter effect becomes more pronounced as the excitation amplitude increases.

Acknowledgement—The authors gratefully acknowledge support for this research by National Science Foundation grant NSF 79 19873. Computational services were provided by the Computer Center of the University of Illinois at Chicago Circle.

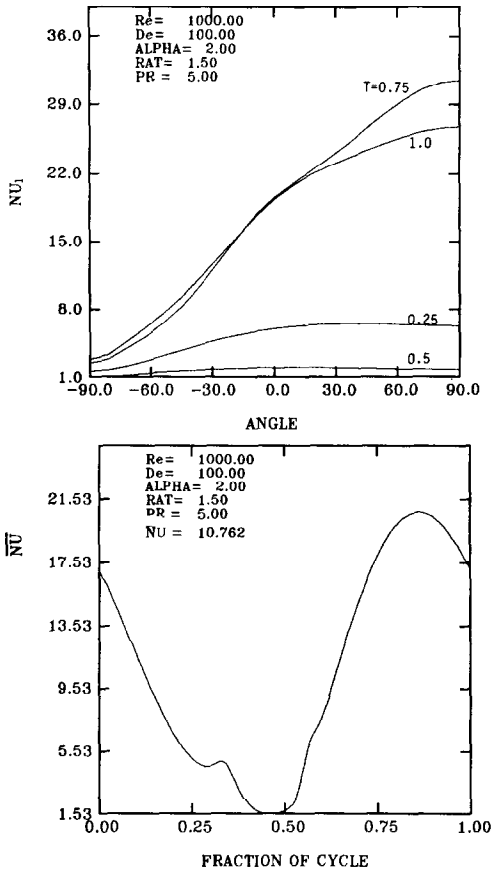

FIG. 9. Local Nusselt number Nu_1 as a function of angle ϕ ($\phi = 90°$ at outside of horizontal diameter) for $T = 0$ (1.0), 0.25, 0.5, 1.0 and peripherally averaged Nusselt number $\overline{Nu}$ as a function of cycle fraction for $\alpha = 2.0$, $k = 1.5$, $Pr = 5.0$, $Re = 1000$ and $De = 100$.

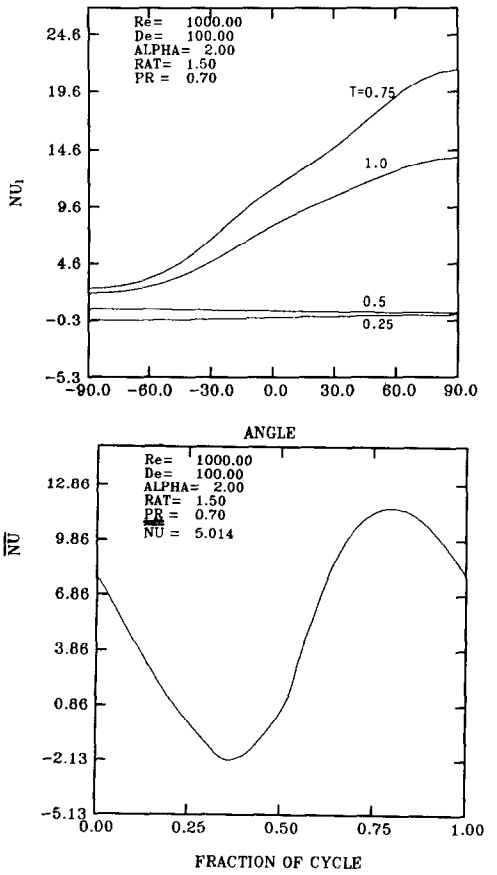

FIG. 10. Local Nusselt number Nu_1 as a function of angle ϕ, ($\phi = 90°$ at outside of horizontal diameter) for $T = 0$ (1.0), 0.25, 0.5, 1.0 and peripherally averaged Nusselt number $\overline{Nu}$ as a function of cycle fraction for $\alpha = 2.0$, $k = 1.5$, $Pr = 0.7$, $Re = 1000$ and $De = 100$.

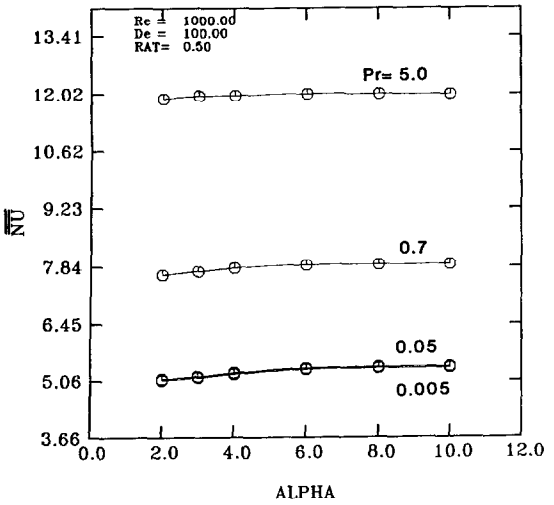

FIG. 11. Time averaged peripherally averaged Nusselt number $\overline{\overline{Nu}}$ as a function of α and Pr for $Re = 1000$, $De = 100$ and $k = 0.5$.

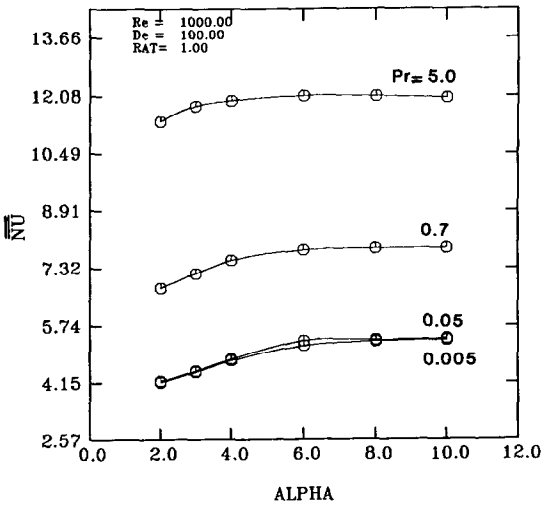

FIG. 12. Time averaged, peripherally averaged Nusselt number $\overline{\overline{Nu}}$ as a function of α and Pr for $Re = 1000$, $De = 100$ and $k = 1.0$.

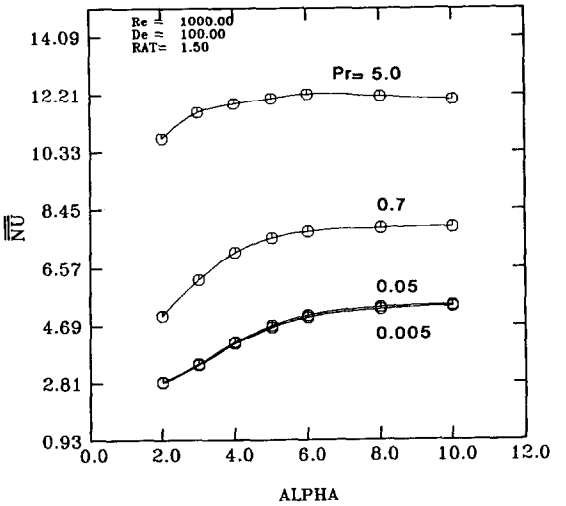

FIG. 13. Time averaged, peripherally averaged Nusselt number $\overline{\overline{Nu}}$ as a function of α and Pr for $Re = 1000$, $De = 100$ and $k = 1.5$.

Table 1. The frozen condition results for $\overline{\overline{Nu}}$ compared to steady state results obtained by Kalb [7]

Pr	Present work (frozen conditions)	Kalb (1973)	Difference (%)
5.0	12.0028	11.10	7.5
0.7	7.8882	7.704	2.3
0.05	5.3968	5.336	1.12
0.005	5.3626	5.306	1.05

REFERENCES

1. W. H. Lyne, Unsteady viscous flow in a curved pipe, *AIChE Jl* **1**, 13–31 (1970).
2. R. Zalosh and W. G. Nelson, Pulsating flow in a curved tube, *J. Fluid Mech* **59**, 693–705 (1973).
3. J. C. F. Chow and C. H. Li, Oscillatory flow in curved tube, *ASCE Engng Mech. Specialty Conf., Waterloo, Canada* (1976).
4. H. A. Simon, M. H. Chang and J. C. F. Chow, Heat transfer in curved tubes with pulsatile, fully developed, laminar flows, *ASME J. Heat Transfer* **99**, 590–595 (1977).
5. N. J. Rabadi, H. A. Simon and J. C. F. Chow, Numerical solution for fully developed, Laminar pulsating flow in curved tubes, *Num. J. Heat Transfer* **3**, 225–239 (1980).
6. N. J. Rabadi, Pulsating flow and heat transfer in curved tubes. Ph.D. thesis, Univ. of Illinois at Chicago Circle (1980).
7. S. P. N. Singh and K. J. Bell, Laminar flow heat transfer in a helically coiled tube, *5th Int. Heat Transfer Conf., Tokyo, Japan*, pp. 193–197 (1974).
8. M. A. Abul-Hamayel, Heat transfer in helically coiled tubes with laminar flow. Ph.D. thesis, Oklahoma State University, Sillwater, Oklahoma (1979).
9. L. S. Yao, and S. A. Berger, Flow in heated curved pipes, *J. Fluid Mech.* **88**, 339–354 (1978).
10. C. E. Kalb, Viscous flow heat transfer in curved tube. Ph.D. thesis, Univ. of Utah (1973).

TRANSFERT THERMIQUE DANS DES TUBES COURBES AVEC UN ECOULEMENT PULSE

Résumé—On étudie les effets d'un écoulement pulsé sur le transfert thermique pour un écoulement pleinement développé, laminaire dans des tubes courbes. Les conditions aux limites thermiques sont un flux pariétal constant axialement avec une température pariétale uniforme sur la périphérie. La distribution de température et les nombres de Nusselt locaux ou moyens sur la périphérie sont calculés pour différentes valeurs de la fréquence, du taux de pulsation, du nombre de Reynolds, du rapport de courbure, des nombres de Dean et de Prandtl. Les résultats montrent qu'il y a une variation considérable des nombres de Nusselt locaux ou moyens sur la périphérie. Le nombre de Nusselt moyenné dans le temps et l'espace approche le cas correspondant permanent lorsque le paramètre de fréquence est $\alpha = 6$ et il décroit lorsque α diminue. Une diminution est associée à l'augmentation du taux de pulsation aux basses fréquences.

WÄRMETRANSPORT IN GEKRÜMMTEN ROHREN BEI PULSIERENDER STRÖMUNG

Zusammenfassung—Es werden Einflüsse der pulsierenden Strömung auf die Wärmetransport-Eigenschaften bei voll ausgebildeter laminarer pulsierender Strömung in gekrümmten Rohren untersucht. Als Randbedingung wird ein gleichmäßiger Wärmestrom in der axialen Richtung mit konstanter Wandtemperatur über den Umfang angenommen. Temperaturverteilung und sowohl lokale als auch über den Umfang gemittelte Nusselt-Zahlen werden für verschiedene Frequenz- und Amplituden-Verhältnisse, Reynolds-Zahlen, Krümmungsradien-Verhältnisse, Dean- und Prandtl-Zahlen ermittelt. Das Ergebnis zeigt einen beträchtlichen Unterschied zwischen der lokalen und der über den Umfang gemittelten Nusselt-Zahl. Die zeitlich und räumlich gemittelte Nusselt-Zahl nähert sich derjenigen der entsprechenden stationären Strömung bei einem Frequenzparameter von $\alpha = 6$ und fällt mit abnehmendem α. Eine weitere Abnahme ist mit einem steigenden Amplitudenverhältnis bei niedrigen Frequenzen verbunden.

ТЕПЛОПЕРЕНОС В ИСКРИВЛЕННЫХ ТРУБАХ ПРИ ПУЛЬСИРУЮЩЕМ ТЕЧЕНИИ

Аннотация — Влияние пульсаций на характеристики теплообмена исследуется при полностью развитом ламинарном и пульсирующем течении жидкости в искривленных трубах. В качестве граничных условий теплообмена приняты аксиально равномерный тепловой поток и однородная температура стенки трубы по окружности. Распределение температуры, а также локальные и усредненные по окружности значения числа Нуссельта рассчитываются при различных значениях частоты и отношения амплитуд, числа Рейнольдса, отношения кривизны, а также чисел Дина и Прандтля. Полученные результаты свидетельствуют о существенном изменении локальных и усредненных по окружности значений числа Нуссельта. Усредненные по пространству и времени значения числа Нуссельта при частотном параметре $\alpha = 6$ близки соответствующим значениям для равномерного потока и убывают с уменьшением α. Дальнейшее уменьшение числа Нуссельта при низких частотах связано с ростом отношения амплитуд.